Journal of Materials Science: Materials in Electronics (2018) 29:4096–4105
https://doi.org/10.1007/s10854-017-8354-8

Effects of nanoparticles on the thermal, microstructural and mechanical properties of novel Sn3.5Ag0.5Zn composite solders

C. L. Chuang[1,2] · L. C. Tsao[3]

Received: 2 October 2017 / Accepted: 29 November 2017 / Published online: 4 December 2017
© Springer Science+Business Media, LLC, part of Springer Nature 2017

Abstract

The effects of added nanoparticles (i.e., Al_2O_3 and TiO_2) on the thermal, microstructural and mechanical properties of Sn3.5Ag0.5Zn nanocomposite solders have been investigated. Adding nanoparticles to the Sn3.5Ag0.5Zn solder increases the melting temperature by only 2.1–4.6 °C. It was also confirmed that the nanoparticles affect the microstructural and mechanical properties. The UTS, 0.2 YS, and microhardness of the Sn3.5Ag0.5Zn nanocomposite solder improved, which could be attributed to the refinement of the β-Sn grain size, the precipitation of Ag_3(Sn, Zn) grains, and the second phase dispersion strengthening mechanism. The fracture mechanism of Sn3.5Ag0.5Zn nanocomposite solders was confirmed to be the ductile fracture mode. The cracks were initiated at the interfaces between β-Sn(Zn) grains and Ag(Zn, Sn) phases.

1 Introduction

Solder materials play decisive roles in the reliability of joints in microelectronic packaging because they provide electrical, thermal and mechanical continuity in the electronics industry [1, 2]. Sn-based Pb-free Sn–Ag–Cu (SAC) ternary eutectic (T_{eut} = 217 °C) solders, such as Sn4Ag0.5Cu (SAC405) or Sn3.5Ag0.5Cu (SAC355) alloys, have been widely studied [3, 4]. However, in these solders, the growth of large primary phases of Ag_3Sn [5] and a thick layer of Cu_6Sn_5 intermetallic compounds (IMCs) [6] is often reported to influence the performance and reliability of solder joints. The IMCs formed during soldering have low ductility, and it is this interface that exhibits brittle failure behavior in tests [7]. Researchers have reported that a small addition of Zn to the Pb-free Sn–Ag alloy could reduce its melting point and improve its mechanical performance at no cost to the ductility and wettability [8, 9]. The addition of Zn also increased the oxygen resistance of the Sn–Ag solder due to the formation of Ag–Zn IMCs [10]. Therefore, the Sn–Ag–Zn solder holds promise for the further development of lead-free solders. Recently, it has been proposed that, to improve the reliability of Pb-free solder joints, the IMCs size should be refined and minor non-reacting, non-coarsening, nano-sized reinforcing particles should be added to Sn-based solder, e.g., Al_2O_3 [11], TiO_2 [12–14], SWCNT [15], SiC [16] Fe_2O_3 [17], La_2O_3 [18], POSS [19], Y_2O_3 [20], ZnO [21] and $SrTiO_3$ [22]. Such changes would enhance the microstructural stability, creep resistance, wettability, and mechanical properties of lead-free solders [23]. Tsao et al. [11, 12] reported the influences of nanoparticle reinforcement on the mechanical properties and wettability of SAC nanocomposite solders due to the addition of TiO_2 and Al_2O_3 nanoparticles. The nanoparticles apparently reduce the surface energy and hinder the Cu_6Sn_5 growth [24, 25]. Huang et al. introduced TiO_2 nanoparticles into a novel low-Ag Sn1.5Sb0.7Cu solder matrix and found that TiO_2 nanoparticles effectively impeded the growth of primary Ag_3Sn IMCs [14]. Wang et al. [16] showed that adding nano-SiC into the Sn3.7Ag0.9Zn alloy melt prompts the formation of primary β-Sn phase in the solidified structure. Hammad and Ibrahiem [21] performed indentation creep experiments at room temperature on Sn3.0Ag0.5Cu alloys with 0.7 wt% ZnO nanoparticles concentrations.

✉ L. C. Tsao
tlclung@mail.npust.edu.tw

[1] Department of Occupational Safety and Health, Chung Shan Medical University, No. 110, Sec.1, Chien-Kuo N. Road, Taichung 402, Taiwan

[2] Department of Medical Research, Chung Shan Medical University Hospital, No. 110, Sec.1, Chien-Kuo N. Road, Taichung 402, Taiwan

[3] Graduate Institute of Materials Engineering, National Pingtung University of Science & Technology, 1, Hseuhfu Road, Neipu 91201, Pingtung, Taiwan

This work aimed to investigate the effects of reinforcing nanoparticles (Al_2O_3 and TiO_2) on the thermal, microstructural, and mechanical properties of Sn3.5Ag0.5Zn nanocomposite solder.

2 Experimental details

2.1 Processing of composite solder

In the present study, Sn3.5Ag0.5Zn (SAZ) nanocomposite solder containing 0.5 wt% nanoparticles was used. In previous work, addition of 0.5 wt% nanoparticles on the microstructure and the tensile strength of the nanocomposite solders were improved as well [11–13]. The SAZ solder matrix was prepared from bulk pure Sn, Ag and Zn rods (all with a purity of 3N5). The SAZ composite solder mixture was prepared by mechanically combining nano-particles (e.g., 20 nm-TiO_2 and 100 nm-Al_2O_3, Nanostructured & Amorphous materials, USA) with Sn3.5Ag0.5Zn solder, followed by remelting in a vacuum furnace at 650 °C for 2.5 h and solidification in steel molds to form squares of 8 × 10 × 20 mm. The mixing procedure of the bulk composite solder has been described in our previous work [14]. Table 1 presents the chemical compositions of the solders studied (wt%).

2.2 Microstructural and DSC characterization

For observation of the microstructures, the SAZ composite solder was etched slightly with 4% HNO_3-96% C_2H_5OH solution for 25 s after mechanical cutting and polishing. The microstructures of the alloys were observed by optical microscopy (OM) and scanning electron microscopy (SEM, S-3000H, Hitachi Co.). The elemental distribution was evaluated by energy dispersive spectroscopy (EDS). X-ray diffraction (XRD, D/max 2500 V/PC) was used to analyze the phases. The phases of the composite solders were determined by X-ray diffraction (XRD) at 20 mA and 40 kV using Cu Ka radiation with diffraction angles of 20°–80° with a constant scanning speed of 0.5 ° min^{-1}. The melting temperatures of the composite solder were defined by differential scanning calorimetry (DSC). The DSC samples, 0.1 mm-thick alloy pieces, were cut from the alloy ingot. Samples were heated from 50 to 260 °C in an Ar atmosphere with heating and cooling rates of 10 °C min^{-1}.

Table 1 Designated composited of the SAZ nanocomposite solder

Sample	Element content (wt%)			
	Ag	Zn	Nanoparticles	Sn
SAZ	3.5	0.5	–	Bal
SAZ-0.5Al_2O_3	3.5	0.5	0.5 (Al_2O_3)	Bal
SAZ-0.5TiO_2	3.5	0.5	0.5 (TiO_2)	Bal

2.3 Mechanical property analysis

Microhardness was determined using an automatic digital microhardness tester with a 10 gf indenting load and a load dwell time of 15 s. For each specimen, five points were tested, and arithmetical mean values were obtained. Tensile tests were performed on samples with a dog-bone shape and a gage section of 2 mm × 3 mm × 8 mm at a constant strain rate of 1×10^{-2} s^{-1} at room temperature.

3 Results and discussion

3.1 DSC testing

Figure 1 shows the DSC curves of SAZ nanocomposite solders. The solidus temperatures (T_S), liquidus temperatures (T_L), and melting ranges ($\Delta T = T_L - T_S$) of the SAZ nanocomposite solders are presented in Table 1. Figure 1a shows the DSC traces of SAZ without any reinforcement addition. It can be seen that the SAZ solder was a eutectic alloy with a solidus temperature (T_S) of 218.2 °C and liquidus temperature (T_L) of 227.6 °C. The melting range ($\Delta T = T_L - T_S$) was 9.5 °C. Figure 1b, c show the DSC traces of SAZ nanocomposite solders reinforced with 0.5 wt% of Al_2O_3 and TiO_2, respectively. The T_S range of the SAZ nanocomposite solders (217.9–224.5 °C) was similar to that of the SAZ solder. It is obvious that the T_L and ΔT of the SAZ nanocomposite solders were below those of the SAZ solder, especially those of the SAZ-0.5TiO_2 nanocomposite solder. It has been reported that the addition of a small quantity of nanoparticles slightly decreases both the liquidus temperatures and melting ranges of nanocomposite solders (Table 2) [26–28]. Lie et al. reported that adding trace nano-SiC reduces the liquidus temperature of Sn3.8Ag0.7Cu solder [28].

To simplify the reasons for the changes, (i) the nanoparticles Al_2O_3 and TiO_2 have a higher surface free energy; (ii) the addition of a small percentage of nanoparticles slightly increases the surface instability of the nanocomposite solder. Also, the non-reacting, non-coarsening, nano-sized nanoparticles can significantly alter the grain boundary/interfacial characteristics of the nanocomposite solders to induce these changes in physical properties. As a result, both the T_L and ΔT of the SAZ nanocomposite solders are decreased.

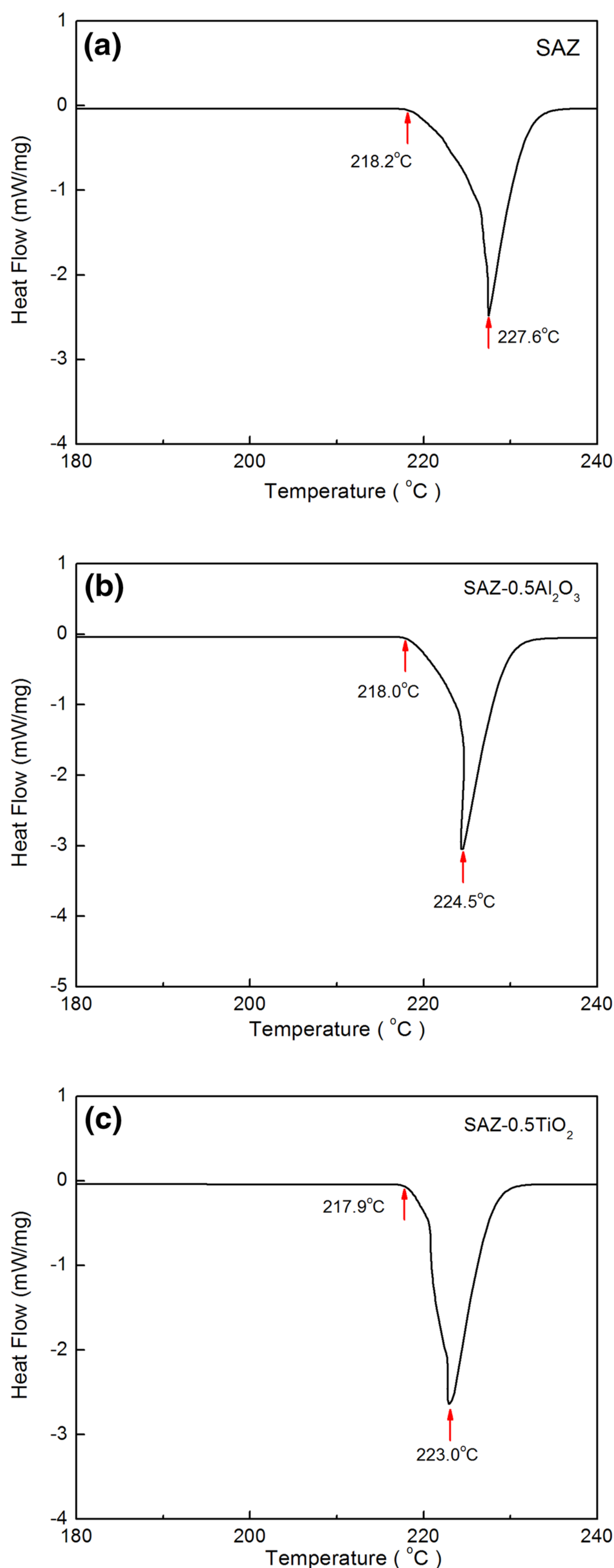

Fig. 1 DSC curves of the as-cast solders: **a** SAZ solder, **b** SAZ-0.5Al_2O_3 nanocomposite solder; **c** SAZ-0.5TiO_2 nanocomposite solder

3.2 Microstructures of solder alloys

Figure 2 shows OM images of the SAZ nanocomposite solders. As shown in Fig. 2a, the microstructure of SAZ solder consisted of white *β*-Sn and black IMCs/Sn eutectic areas. Comparing Fig. 2b–c, it can be seen that the addition of nanoparticles (i.e., Al_2O_3 and TiO_2) into the SAZ solder influenced the microstructures of the nanocomposite solders significantly. The size of the IMCs phase in the eutectic area was refined obviously by the addition of nanoparticles. The SEM micrograph of the SAZ solder shown in Fig. 3a shows *β*-Sn(Zn) (mark 1, EDS analysis see Table 3), Ag_3(Sn, Zn)/Sn(Zn) eutectic areas (mark 2), and a small portion of Ag(Zn, Sn) phase in the solidified SAZ solder. According to Refs. [29–31], the composition of the Sn–Ag–Zn solder was β-Sn, Ag_3Sn, ζ-AgZn and β′-AgZn, respectively. Referring to the binary Sn–Ag phase diagram and ternary Sn–Ag–Zn phase diagram, Fig. 4 presents the schematic diagram of SAZ solders [29, 32].

It can be noticed that some fiber-like rich Ag of Ag(Zn, Sn) phases (mark 3) were separated along the sub-grain boundaries, and the large dot-like Ag(Zn, Sn) grains (mark 4) were embedded in the solder matrix. EDS analysis (see Fig. 5) showed that the percentages of Ag and Zn (wt%) were about 60.2:38.5. XRD was conducted to identify the phase structures of the SAZ, SAZ-0.5Al_2O_3 and SAZ-0.5TiO_2 solders, and the corresponding patterns are presented in Fig. 6. In Fig. 6a, the Ag_3(Sn, Zn), β′-Ag(Zn, Sn) and the β-Sn(Zn) phases were detected in SAZ solder.

These results further indicate that the SAZ solder followed the pseudo eutectic reaction [29–34]:

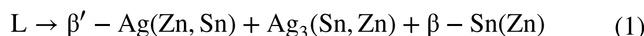

$$L \rightarrow \beta' - Ag(Zn, Sn) + Ag_3(Sn, Zn) + \beta - Sn(Zn) \quad (1)$$

When nano-Al_2O_3 particles were added to the SAZ solder (Table 3), the chemical composition (wt%) of the eutectic areas contained Sn (84.8%), Ag (5.1%), Zn (1.2%), Al(3.1%) and O (5.8%). In the SAZ nanocomposite solder, the XRD profile indicated the additional presence of minor amounts of nano-Al_2O_3 particles (Fig. 4b). Therefore, the nano-Al_2O_3 particles were successfully mixed with the SAZ nanocomposite solder. As shown Fig. 3b, the addition of nano-Al_2O_3 particles influenced the microstructure of SAZ nanocomposite solder, and the size and spacing of Ag_3(Sn, Zn) grains decreased significantly. In addition, neither large Ag(Zn, Sn) nor large Ag_3(Sn, Zn) grains were observed in the SAZ-0.5Al_2O_3 nanocomposite solder. The same phenomenon was also observed in the SAZ-nano-TiO_2 nanocomposite solders (Fig. 4c). In short, due to the adsorption effect and high surface free energy of the nanoparticles (i.e., Al_2O_3 and TiO_2) on the grain surface, the growth of IMCs grains was suppressed during the solidification process [11].

Table 2 Solidus, liquidus, and melting range of the SAZ nanocomposite in this study

Samples	Nanaparticles		Solidus, T_S, °C	Liquidus, T_L °C	ΔT (=T_L–T_s)	Ref.
	wt%	Type				
SAZ	–	–	218.2	227.6	9.4	
SAZ-0.5Al_2O_3	0.5	Al_2O_3	218.0	224.5	6.5	
SAZ-0.5TiO_2	0.5	TiO_2	217.9	223.0	5.1	
Sn9Zn	–	–	198.5	202.1	–	
Sn9Zn-0.5Al_2O_3	0.5	Al_2O_3	198.4	201.7	–	[21]
Sn9Zn-1Al_2O_3	1	Al_2O_3	197.8	201.2	–	
Sn0.7Cu	–	–	226.50	229.67	3.17	[22]
Sn0.7Cu-0.25TiO_2	0.25	–	226.21	229.24	3.03	
Sn0.7Cu-0.5TiO_2	0.5	–	226.24	229.10	2.86	
Sn0.7Cu-1TiO_2	1	–	226.17	228.82	2.65	
Sn3.8Ag0.7Cu	–	–	–	219.9	–	[23]
Sn3.8Ag0.7Cu-0.01SiC	0.01	SiC	–	219.2	–	
Sn3.8Ag0.7Cu-0.05SiC	0.05	SiC	–	219.0	–	
Sn3.8Ag0.7Cu-0.20SiC	0.2	SiC	–	218.9	–	

According to the adsorption theory of nanoparticles (i.e., Al_2O_3 and TiO_2), the surface free energy of IMCs [i.e., Ag_3(Sn, Zn) and Ag(Zn, Sn)] grains is:

$$\sum_K \gamma_c^K A_K = \sum_K (\gamma_o^K - RT \int_o^c \frac{\Gamma^K}{c} dc) A_K \quad (2)$$

$$= \sum_K \gamma_o^K A_K - RT \sum_K A_K \int_o^c \frac{\Gamma^K}{c} dc \rightarrow \min \quad (3)$$

where Γ^K is the amount of adsorption of nanoparticles at the IMCs grains K, c is the concentration of nanoparticles (i.e., Al_2O_3 and TiO_2), R is the Plank constant, T is the absolute temperature, γ^K is the surface tension of IMCs grains K, γ_c^K is the surface tension of the IMCs grains K with adsorption of nanoparticles, γ_o^K is the surface tension of IMCs grains K without adsorption of nanoparticles, and A_K is the area of IMCs grains K. Given that the volume is constant, the surface energy of the planes must be kept to a minimum in the equilibrium state. Here, $\sum_K \gamma_o^K A_K$ is assumed to be constant because it is independent of the concentration of nanoparticles. That is,

$$\sum_K A_K \int_o^c \frac{\Gamma^K}{c} dc \rightarrow \max, \quad (4)$$

This implies that the effect on the grain boundaries of the IMCs grains with the maximum Γ^K value is most active.

During the solidification process, when Ag_3(Sn, Zn) and/or Ag(Zn, Sn) grains had a relatively large surface tension and grew rapidly, their surfaces had a maximum adsorption of active nanoparticles, and thus the surface energy of the Ag_3(Sn, Zn) and/or Ag(Zn, Sn) grains decreased. Therefore, the growth rate of IMCs grains was suppressed, resulting in a refined Ag_3(Sn, Zn) and/or Ag(Zn, Sn) phase.

It is quite difficult to calculate the surface energy in order to minimize the free energy of the entire SAZ nanocomposite solder. As shown by the OM and SEM in Figs. 2 and 3, the sizes of the IMCs grains decreased in the SAZ nanocomposite solders.

3.3 Microhardness measurements

The Vickers microhardness values represent the average microhardness values of five indents performed on the different SAZ nanocomposite solders. The error bars are presented to represent standard deviation. Results obtained from the Vickers microhardness test on the SAZ nanocomposite solders are shown in Table 4. The microhardness results are compared in Fig. 7. The microhardness values of the SAZ and the SAZ-0.5Al_2O_3 and SAZ-0.5TiO_2 nanocomposite solders were 15.5 ± 0.6, 18.1 ± 0.5, and 18.8 ± 0.6 Hv, respectively. It can be seen from Table 4 that the SAZ nanocomposite solders had higher microhardness values (about 16.8% for Al_2O_3 and 21.3% for TiO_2, respectively) owing to the homogeneous distribution of nanoparticles in the solder matrix, and the refined compounds of Ag_3(Sn, Zn) and Ag(Zn, Sn) IMCs grains could act as reinforcement [11, 13].

3.4 Tensile testing

Figure 8 presents the typical tensile stress–strain curves of the SAZ nanocomposite solder at a constant strain rate of 1×10^{-2} s^{-1} at room temperature. The analysis tests

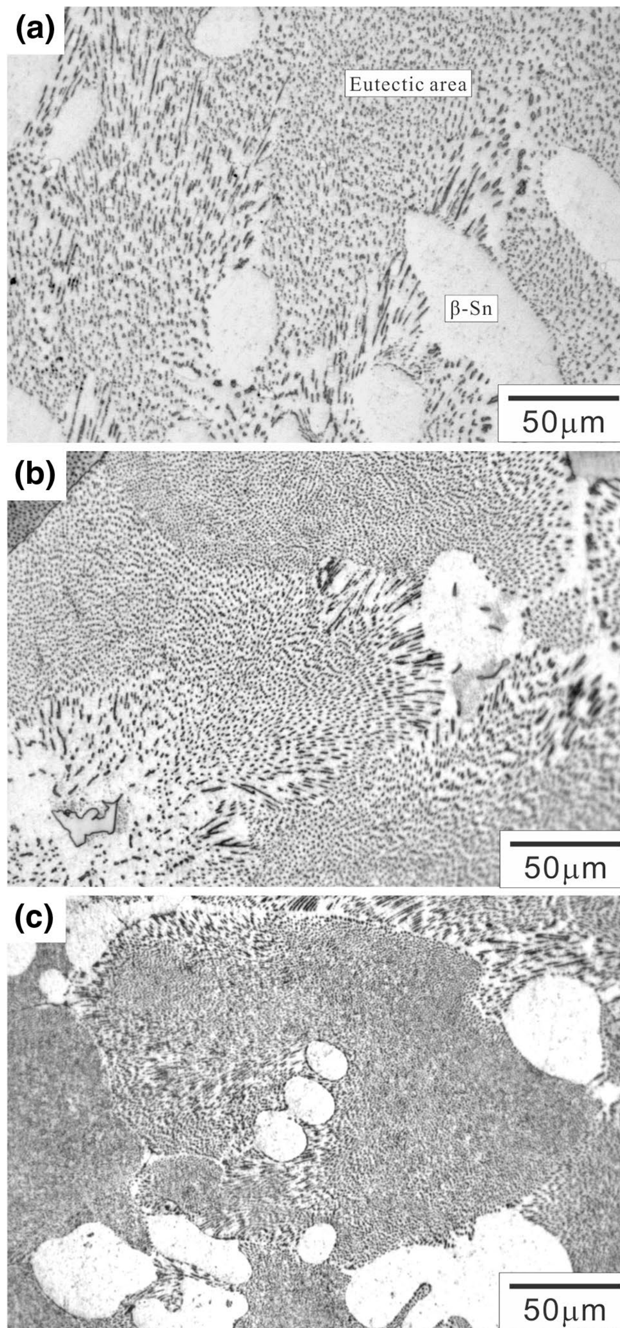

Fig. 2 Optical micrographs showing the microstructures of solders: **a** SAZ solder, **b** SAZ-0.5Al_2O_3 nanocomposite solder; **c** SAZ-0.5TiO_2 nanocomposite solder

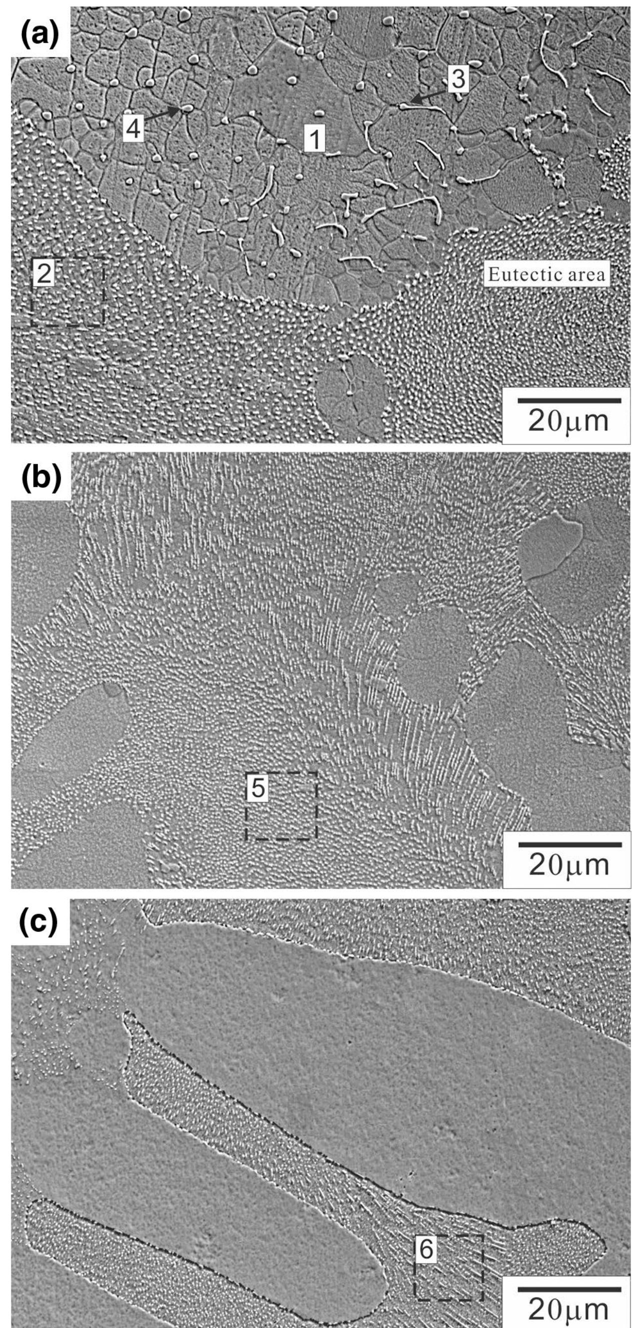

Fig. 3 SEM micrographs of as-cast solders: **a** SAZ solder, **b** SAZ-0.5Al_2O_3 nanocomposite solder; **c** SAZ-0.5TiO_2 nanocomposite solder

were conducted on four different samples taken from the same solder, and the average values of the ultimate tensile strength (UTS), 0.2% yield strength (0.2 YS) and percentage of elongation are given in Table 5. The average UTS values were 39.8 ± 5.1, 46.1 ± 7.7 and 50.3 ± 6.6 MPa; the average 0.2 YS values were 32.8 ± 6.3, 43.9 ± 5.2 and 45.1 ± 6.4 MPa; and the average elongation percentages were 79.4 ± 6.3, 70.1 ± 5.3 and 59.3 ± 5.8% for the SAZ, SAZ-0.5Al_2O_3 and SAZ-0.5TiO_2 solders, respectively. Regarding the addition of nanoparticles (Table 6), the UTS and 0.2 YS of the SAZ nanocomposite solders were higher (+ 15.8 and 33.8% for the SAZ-0.5Al_2O_3 nanocomposite solder; + 26.4 and 37.5% for the SAZ-0.5TiO_2 nanocomposite solder, respectively) than those of the SAZ

Table 3 EDS analysis results of site indicated in Fig. 3

Site	Element (wt%)						Phase
	Sn	Ag	Zn	Ti	Al	O	
1	99.1	0.9	–	–	–	–	*β*-Sn(Zn)
2	88.6	8.7	2.7	–	–	–	Eutectic area, *β*-Sn(Zn) + Ag_3(Sn, Zn)
3	5.3	58.9	35.8	–	–	–	Fiber-like Ag(Zn, Sn)
4	1.3	60.2	38.5	–	–	–	Dot-like Ag(Zn, Sn)
5	84.8	5.1	1.2	–	3.1	5.8	Eutectic area, *β*-Sn(Zn) + Al_2O_3
6	82.6	4.1	1.3	2.3	–	6.1	Eutectic area, *β*-Sn(Zn) + TiO_2

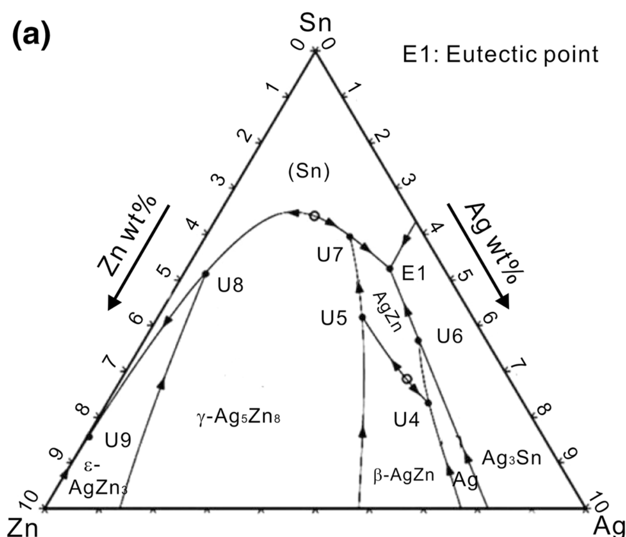

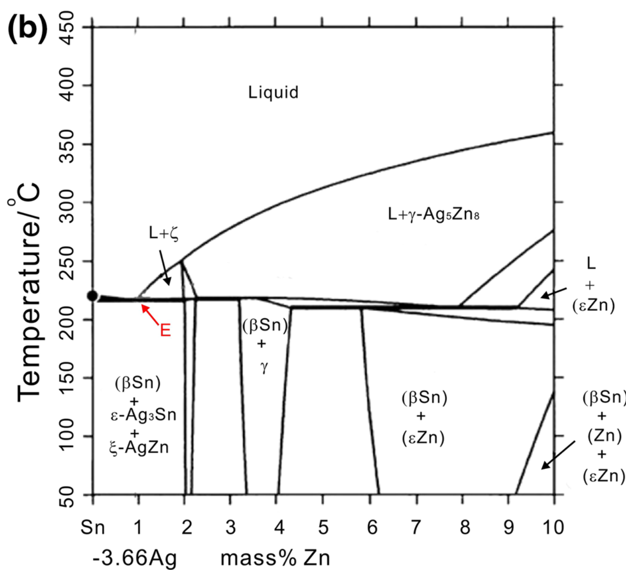

Fig. 4 Phase diagram of **a** Sn–Ag–Zn ternary alloy [29] and **b** at the vertical section [32]

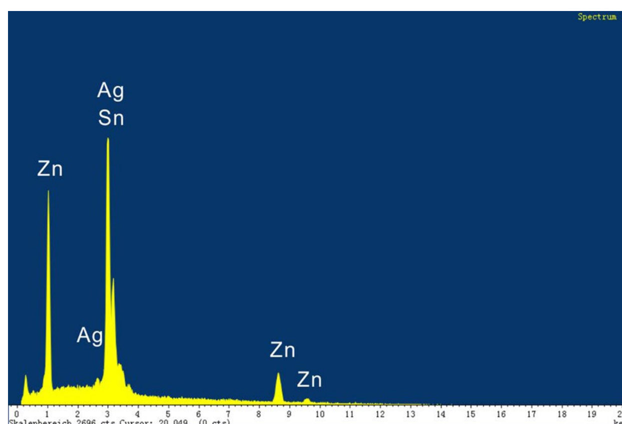

Fig. 5 EDS analysis results of the company island eutectic area in Fig. 3

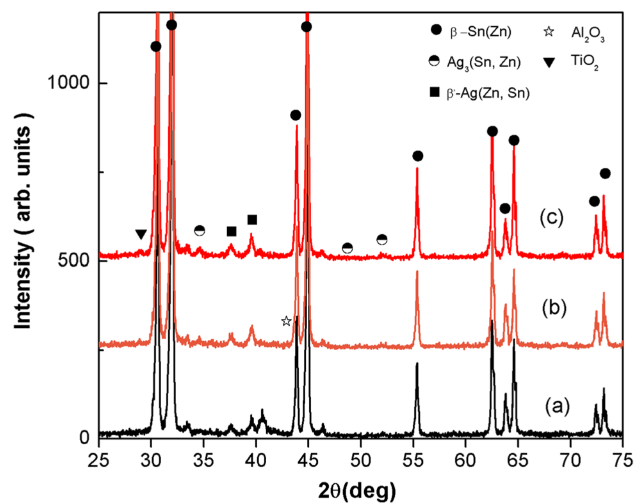

Fig. 6 XRD analysis of *a* SAZ solder; *b* SAZ-0.5Al_2O_3 composite solder; *c* SAZ-0.5TiO_2 composite solder

solder. It should also be noted that the elongation ratios were much lower for the nanocomposite solders (−11.7% for SAZ-Al_2O_3 and −25.3% for SAZ-TiO_2) than for the SAZ solder. It is obvious that the nanoparticles affected the microstructure and mechanical properties. This

Table 4 Microhardness measurements of the SAZ nanocomposite solders

Sample	Microhardness indention results (Hv)						
	Trial 1	Trial 2	Trial 3	Trial 4	Trial 5	Average	Adding ration
SAZ	15.8	16.1	15.0	14.9	15.6	15.5 ± 0.6	–
SAZ-0.5Al_2O_3	18.2	18.6	17.9	17.8	18.2	18.1 ± 0.5	+ 16.8
SAZ-0.5TiO_2	18.2	18.9	18.7	19.3	18.9	18.8 ± 0.6	+ 21.3

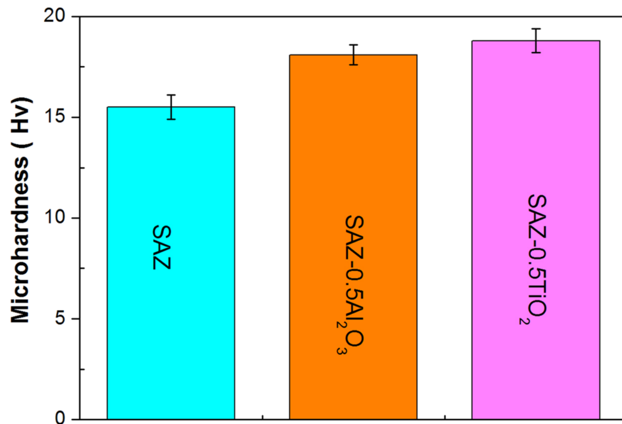

Fig. 7 Measured microhardness values of the SAZ nanocomposite solders

improvement of mechanical behavior is mainly attributed to the fine β-Sn(Zn) dendrites, the precipitation of Ag_3(Sn, Zn) and Ag(Zn, Sn) grains, and the second phase dispersion strengthening mechanism. This finding is consistent with previously reported results [2]. Many reported that significant improvement in the microhardness, UTS and 0.2% YS of the composite solders due to the presence of the second phases (nano-IMCs and nanoparticles). Several possible factors can contribute to this strengthening mechanism [13, 27]: (i) $\sigma_{Hall-petch}$, the grain size refinement effect ($\sigma_{Hall-petch}$); (ii) σ_{Orowan}, the Orowan strengthening mechanism due to the presence of nanoparticles (TiO_2 and Al_2O_3) in the composite solder matrix and precipitation to nano size and/or submicro IMCs [Ag_3(Sn, Zn) and Ag(Zn, Sn)]; (iii) σ_{CTE}, the generation of geometrically necessary dislocations to accommodate CTE mismatch between the matrix and the particles; and (iv) σ_{Load}, the load-bearing effects due to the presence of nano-sized reinforcements. So, these main factors can be coupled together to improving the yield strength. Another, previous reports have suggested that high concentrations of micro voids develop along grain boundaries and become crack nucleation sites in second phase particles [12, 24, 35]. Therefore, the elongation of the SAZ nanocomposite solder was slightly lower than that of the SAZ solder [36].

3.5 Fracture analysis

Figure 9 presents the fractured surface morphology of SAZ nanocomposite solders after tensile tests at room temperature (25 °C) and a strain rate of $1 \times 10^{-2}\ s^{-1}$. A number of typical dimple structures were observed in the SAZ nanocomposite solders, representing the ductile fracture mode (Fig. 9a) [37]. It was found that the fracture surface of the SAZ solder was coarse and the Ag(Zn, Sn) IMCs had a dimpled surface (Fig. 9a). In addition, the fracture surface of the nanocomposite solder had a small dimple pattern, and the dimples of the SAZ-0.5TiO_2 nanocomposite solder were smaller. This finding is consistent with the cracks initiating at the interface between Ag(Zn, Sn) and β-Sn(Zn).

4 Conclusions

The effects of added nanoparticles (i.e., Al_2O_3 and TiO_2) on the thermal, microstructural and mechanical properties of SAZ nanocomposite solders have been investigated. Significant conclusions obtained in this research are as follows:

(1) Alloying of 0.5 wt% Al_2O_3 and 0.5 wt% TiO_2 considerably reduces the liquidus temperatures and slightly decreases the melting range of 2.9–4.3 °C, while elevating the melting temperature by about 2.1–4.6 °C.
(2) The addition of nanoparticles to SAZ alloy suppresses the formation of large β-Sn(Zn) grains and large dot/fiber-like precipitates, instead favoring the formation of small β-Sn(Zn) dendrites surrounded by fine eutectic regions of β-Sn(Zn), Ag_3(Sn, Zn), and Ag(Zn, Sn) IMCs.
(3) The UTS, 0.2 YS and microhardness of the SAZ nanocomposite solder improved, which could be attributed to the refinement of the β-Sn(Zn) grain size, the precipitation of Ag_3(Sn, Zn) and Ag(Zn, Sn) grains, and the second phase dispersion strengthening mechanism.
(4) The fracture mechanism of SAZ nanocomposite solders was confirmed to be the ductile fracture mode, and the cracks were initiated at the interface between Ag(Zn, Sn) and β-Sn(Zn).

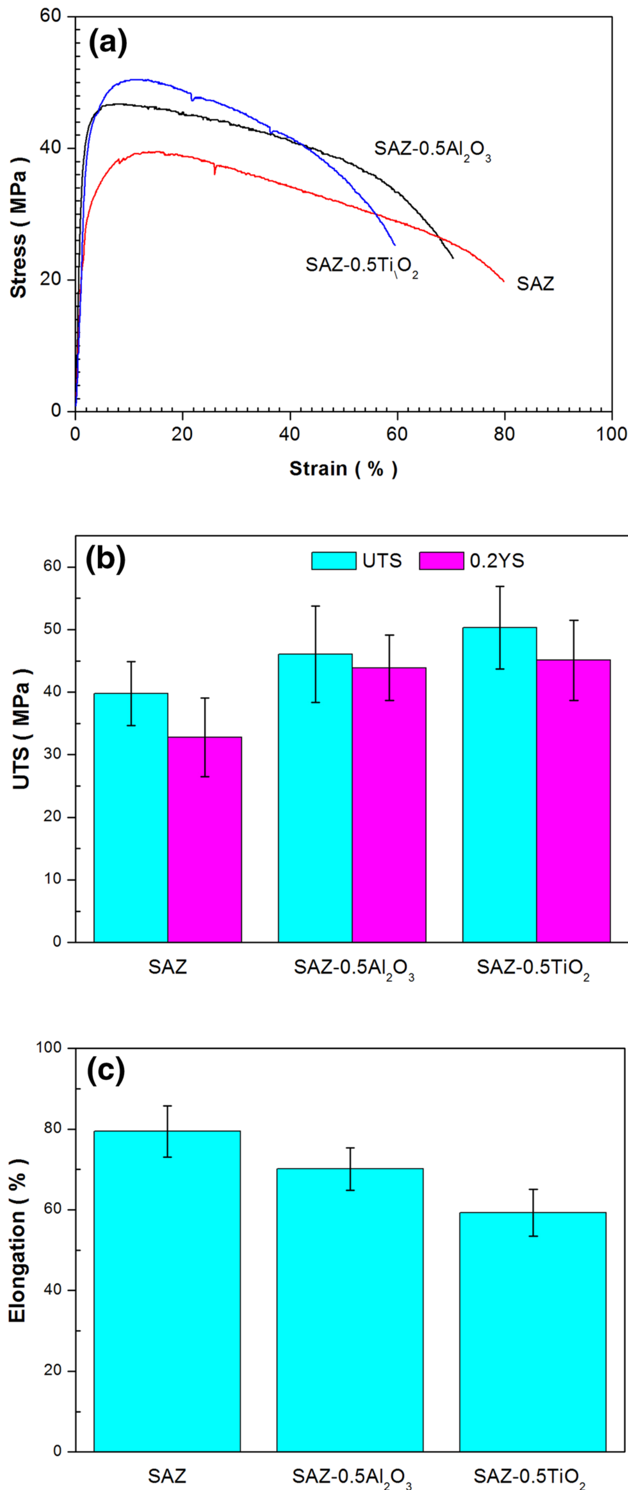

Fig. 8 Tensile stress–strain curves of the lead-free Sn3.5Ag0.5Zn nanocomposite solders at room temperature: **a** SAZ solder; **b** SAZ-0.5Al_2O_3 nanocomposite solder; **c** SAZ-0.5TiO_2 nanocomposite solder

Table 5 Mechanical property for various SAZ nanocomposite solders

Sample	UTS (MPa)	0.2 YS (MPa)	Elongation (%)
SAZ	39.8 ± 5.1	32.8 ± 6.3	79.4 ± 6.3
SAZ-0.5Al_2O_3	46.1 ± 7.7	43.9 ± 5.2	70.1 ± 5.3
SAZ-0.5TiO_2	50.3 ± 6.6	45.1 ± 6.4	59.3 ± 5.8

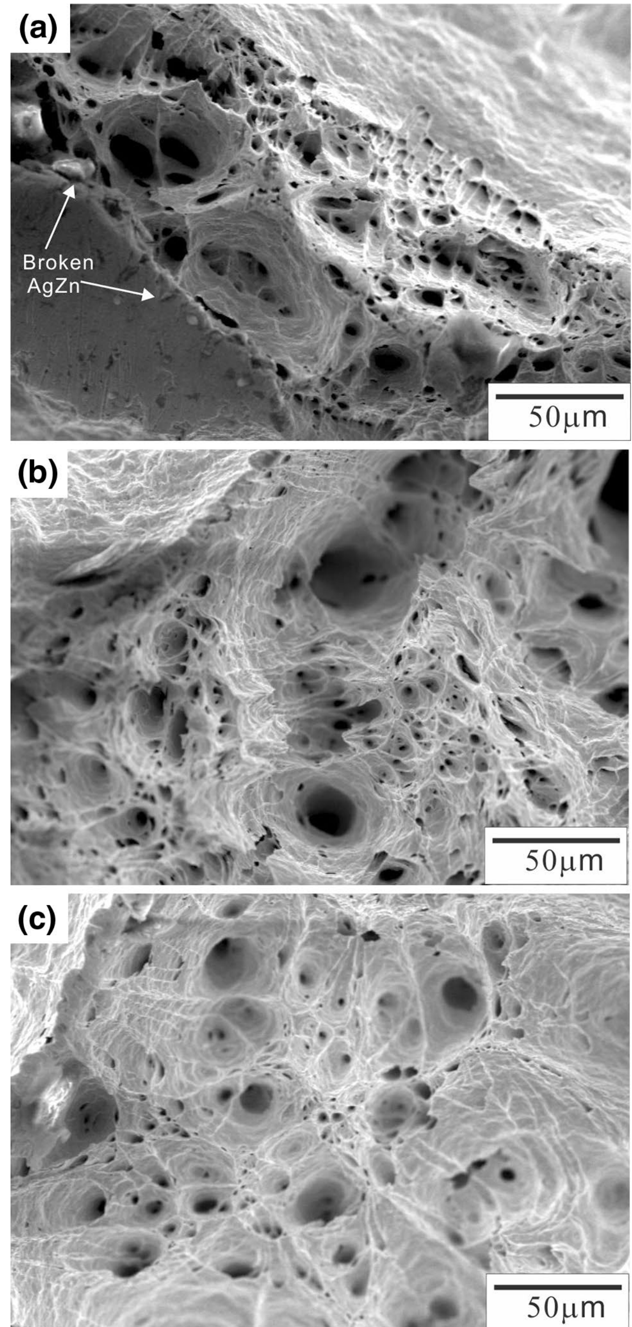

Fig. 9 Tensile fractured microstructures of **a** SAZ solder; **b** SAZ-0.5Al_2O_3 nanocomposite solder; **c** SAZ-0.5TiO_2 nanocomposite solder

Table 6 The relative ratios of UTS, 0.2 YS and elongation of SAZ nanocomposite solders

Solder	UTS	0.2 YS	Elongation
SAZ-0.5Al_2O_3	+15.8	+33.8	−11.7
SAZ-0.5TiO_2	+26.4	+37.5	−25.3

Acknowledgements The authors acknowledge the financial support of this work from the Ministry of Science and Technology, Taiwan, under Project No. MOST 106-2221-E-020-015. SEM was performed by the Precision Instrument Center of National Pingtung University of Science and Technology, Taiwan.

References

1. H.J. Lin, T.H. Chuang, Interfacial microstructure and bonding strength of Sn-3Ag-0.5Cu and Sn-3Ag-0.5Cu-0.5Ce-XZn solder BGA packages with immersion Ag surface finish. Microelectron. Reliab. **51**, 445–452 (2011)
2. L.C. Tsao, R.W. Wu, T.H. Cheng, K.H. Fan, R.S. Chen, Effects of nano-Al_2O_3 particles on microstructure and mechanical properties of Sn3.5Ag0.5Cu composite solder ball grid array joints on Sn/Cu pads. Mater. Des. **50**, 774–781 (2013)
3. N.C. Lee, Lead-free soldering. Mater. Adv. Packag. 199–236 (2016)
4. C.L. Chuang, L.C. Tsao, H.K. Lin, L.P. Feng, Effects of small amount of active Ti element additions on microstructure and property of Sn3.5Ag0.5Cu solder. Mater. Sci. Eng. A **558**, 478–484 (2012)
5. S.K. Kang, W.K. Choi, D.Y. Shih, D.W. Henderson, T. Gosselin, A. Sarkhel, N.Y. Charles Goldsmith, K.J. Puttlitz, W.K. Choi, Ag_3Sn plate formation in the solidification of near-ternary eutectic Sn-Ag-Cu. JOM **55**, 61–65 (2003)
6. S.W. Jeong, J.H. Kim, H.M. Lee, Effect of cooling rate on growth of the intermetallic compound and fracture mode of near-eutectic Sn-Ag-Cu/Cu pad: before and after aging. J. Electron. Mater. **33**, 1530–1544 (2004)
7. W.M. Xiao, Y.W. Shi, Y.P. Lei, Z.D. Xia, F. Guo, Comparative study of microstructures and properties of three valuable SnAgCuRE lead-free solder alloys. J. Electron. Mater. **35**, 1095–1103 (2006)
8. C. Wei, Y.C. Liu, Y.J. Han, J.B. Wan, K. Yang, Effects of aging on structural evolution of the rapidly solidified Sn-Ag-Zn eutectic solder. J. Alloys Compd. **468**, 154–157 (2009)
9. M. McCormack, S. Jin, G.W. Kammlott, H.S. Chen, New Pb-free solder alloy with superior mechanical properties. Appl. Phys. Lett. **63**, 15–17 (1993)
10. S. Knott, H. Flandorfer, A. Mikula, Calorimetric investigations of the two ternary systems Al-Sn-Zn and Ag-Sn-Zn. Z. Metallkd. **96**, 38–44 (2005)
11. L.C. Tsao, S.Y. Chang, C.I. Lee, W.H. Sun, C.H. Chiang, Effects of nano-Al_2O_3 additions on microstructure development and hardness of Sn3.5Ag0.5Cu solder. Mater. Des. **31**, 4831–4835 (2010)
12. L.C. Tsao, S.Y. Chang, Effects of nano-TiO_2 additions on thermal analysis, microstructure and tensile properties of Sn3.5Ag0.25Cu solder. Mater. Des. **31**, 990–993 (2010)
13. T.H. Chuang, L.C. Tsao, C.H. Chung, S.Y. Chang, Evolution of Ag_3Sn compounds and microhardness of Sn3.5Ag0.5Cu nanocomposite solders during different cooling rate and aging. Mater. Des. **39**, 475–483 (2012)
14. C.H. Huang, C.H. Chen, S.Y. Chang, L.C. Tsao, R.S. Chen, Effect of TiO_2 nanoparticle addition and cooling rate on microstructure and mechanical properties of novel Sn1.5Sb0.7Cu solders. J. Mater. Sci.: Mater. Electron. **26**, 3493–3501 (2015)
15. K. Mohan Kumar, V. Kripesh, A.A.O. Tay, Single-wall carbon nanotube (SWCNT) functionalized Sn-Ag-Cu lead-free composite solders. J. Alloys Compd. **450**, 229–237 (2008)
16. X. Wang, Y.C. Liu, C. Wei, H.X. Gao, P. Jiang, L.M. Yu, Strengthening mechanism of SiC-particulate reinforced Sn-3.7Ag-0.9Zn lead-free solder. J. Alloys Compd. **480**, 662–665 (2009)
17. Y. Gu, X.C. Zhao, Y. Li, Y. Liu, Y. Wang, Z.Y. Li, Effect of nano-Fe_2O_3 additions on wettability and interfacial intermetallic growth of low-Ag content Sn-Ag-Cu solders on Cu substrates. J. Alloys Compd. **627**, 39–47 (2015)
18. A. Sharma, B.G. Baek, J.P. Jung, Influence of La_2O_3 nanoparticle additions on microstructure, wetting, and tensile characteristics of Sn-Ag-Cu alloy. Mater. Des. **87**, 370–379 (2015)
19. F. Tai, F. Gao, Z.D. Xia, Y.P. Lei, Y.W. Shi, Effects of nano-structured particles on microstructure and microhardness of Sn-Ag solder alloy. J. Mater. Sci. Mater. Electron. **21**, 702–707 (2010)
20. L.M. Yang, Z.F. Zhang, Effect of Y_2O_3 nanoparticles addition on the microstructure and tensile strength of Cu/Sn3. 0Ag0. 5Cu solder joint. J. Appl. Phys. **117**, 015308 (2015)
21. A.E. Hammad, A.A. Ibrahiem, Enhancing the microstructure and tensile creep resistance of Sn-3.0Ag-0.5Cu solder alloy by reinforcing nano-sized ZnO particles. Microelectron. Reliab. **75**, 187–194 (2017)
22. T. Fouzder, I. Shafiq, Y.C. Chan, A. Sharif, W.K.C. Yung, Influence of $SrTiO_3$ nano-particles on the microstructure and shear strength of Sn-Ag-Cu solder on Au/Ni metallized Cu pads. J. Alloys Compd. **509**, 1885–1892 (2011)
23. L. Zhang, K.N. Tu, Structure and properties of lead-free solders bearing micro and nanoparticles. Mater. Sci. Eng. **R82**, 1–32 (2014)
24. L.C. Tsao, Evolution of nano-Ag_3Sn particle formation on Cu-Sn intermetallic compounds of Sn3.5Ag0.5Cu composite solder/Cu during soldering. J. Alloys Compd. **509**, 2326–2333 (2011)
25. L.C. Tsao, Suppressing effect of 0.5 wt% nano-TiO_2 addition into Sn-3.5Ag-0.5Cu solder alloy on the intermetallic growth with Cu substrate during isothermal aging. J. Alloys Compd. **509**, 8441–8448 (2011)
26. W.Q. Xing, X.Y. Yu, H. Li, L. Ma, W. Zuo, P. Dong, W.X. Wang, M. Ding, Effect of nano Al_2O_3 additions on the interfacial behavior and mechanical properties of eutectic Sn-9Zn solder on low temperature wetting and soldering of 6061 aluminum alloys. J. Alloy Compd. **695**, 574–582 (2017)
27. L.C. Tsao, C.H. Huang, C.H. Chung, R.S. Chen, Influence of TiO_2 nanoparticles addition on the microstructural and mechanical properties of Sn0.7Cu nano-composite solder. Mater. Sci. Eng. A **545**, 194–200 (2012)
28. P. Liu, P. Yao, J. Liu, Effect of SiC nanoparticle additions on microstructure and microhardness of Sn-Ag-Cu solder alloy. J. Electron. Mater. **37**, 874–879 (2008)
29. H. Ohtani, M. Miyashita, K. Ishida, Thermodynamic study of phase equilibria in the Sn-Ag-Zn system. J. Jpn. Instrum. Methods **63**, 685–694 (1999)
30. U.B.öyükS. Engin, H. Kaya, N. Maraşlı, Effect of solidification parameters on the microstructure of Sn-3.7Ag-0.9Zn solder. Mater. Charact. **61**, 1260–1267 (2010)
31. G.P. Vassilev, E. Dobrev, S. Evtimova, J.C. Tedenac, Studies of the phase equilibria in the Ag–Sn–Zn system. J. Alloy Compd. **327**, 285–291 (2001)
32. I. Ohnuma, M. Miyashita, X.J. Liu, H. Ohtani, K. Ishida, Phase equilibria and thermodynamic properties of Sn-Ag based Pb-free solder alloys. IEEE Trans. Electron. Packag. Manuf. **26**, 84–89 (2003)

33. C. Wei, Y.C. Liu, Y.J. Han, J.B. Wan, K. Yang, Microstructures of eutectic Sn-Ag-Zn solder solidified with different cooling rates. J. Alloys Compd. **464**, 301–305 (2008)
34. S. Engin, U. Böyük., N. Maraşlı, Determination of solid-liquid interfacial energy for a solid Sn in equilibrium with a Sn-Ag-Zn eutectic liquid. Curr. Appl. Phys. **11**, 1060–1066 (2011)
35. S.M.L. Nai, J. Wei, M. Gupta, Improving the performance of lead-free solder reinforced with multi-walled carbon nanotubes. Mater. Sci. Eng. A **423**, 166–169 (2006)
36. A.A. El-daly, S.F. Fawzy, M.J. Mansour, Younis, Thermal analysis and mechanical properties of Sn-1.0Ag-0.5Cu solder alloy after modification with SiC nano-sized particles. J. Mater. Sci.: Mater. Electron. **24**, 2976–2988 (2013)
37. J.M. Song, J.J. Lin, C.F. Huang, H.Y. Chuang, Crystallization, morphology and distribution of Ag_3Sn in Sn-Ag-Cu alloys and their influence on the vibration fracture properties. Mater. Sci. Eng. A **466**, 9–17 (2007)